Electronic Supplementary Material (ESI) for Soft Matter.
This journal is © The Royal Society of Chemistry 2016

SUPPORTING INFORMATION

Self-assembled fibrillar networks of a multifaceted chiral squaramide: Supramolecular multistimuli-responsive alcogels

Jana Schiller,[a] Juan V. Alegre-Requena,[a,b] Eugenia Marqués-López,[b] Raquel P. Herrera,[b] Jordi Casanovas,[c] Carlos Alemán[d] and David Díaz Díaz*[a,e]

[a] *Institut für Organische Chemie, Universität Regensburg, Universitätsstr. 31, 93053 Regensburg, Germany. E-mail: David.Diaz@chemie.uni-regensburg.de; Fax: + 49 941 9434121; Tel.: + 49 941 9434373*
[b] *Laboratorio de Organocatálisis Asimétrica, Departamento de Química Orgánica, Instituto de Síntesis Química y Catálisis Homogénea (ISQCH), CSIC-Universidad de Zaragoza, Pedro Cerbuna 12, 50009 Zaragoza, Spain*
[c] *Departament de Química, EPS, Universitat de Lleida, Jaume II 69, 25001 Lleida, Spain*
[d] *Departament d'Enginyeria Química – ETSEIB and Center for Research in Nano-Engineering, Universitat Politècnica de Catalunya, Av. Diagonal 647, 08028 Barcelona, Spain*
[e] *IQAC-CSIC, Jordi Girona 18-26, 08034 Barcelona, Spain*

Contents List

1. Additional experimental details for the synthesis of compounds

General procedure for the preparation of squaramides 5, 6 and 10

To a solution of 3,4-dimethoxy-3-cyclobutene-1,2-dione (**11**) (1.2 or 3 mmol) in MeOH (3-3.75 mL), amine **12b-d** (1.2 or 3 mmol) was added at room temperature. After the corresponding reaction time (t_1), amine **13a**,**b** (1.2 or 3 mmol) was then added dissolved in MeOH (9 or 11.25 mL). After the corresponding reaction time (t_2), the reaction flask was placed in the freezer (-20 ºC) for 30 minutes and the product was purified by filtration.

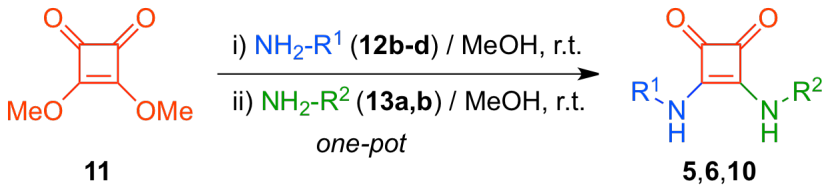

11 **5**,**6**,**10**

5: **12b**/3.75 mL MeOH; **13b**/11.25 mL; t_1 = 3 h, t_2 = 6 h, 86% yield
6: **12c**/3.75 mL MeOH; **13b**/11.25 mL; t_1 = 3 h, t_2 = 7 h, 88% yield
10: **12d**/3 mL MeOH; **13a**/9 mL; t_1 = 2 h, t_2 = 3 h, 74% yield

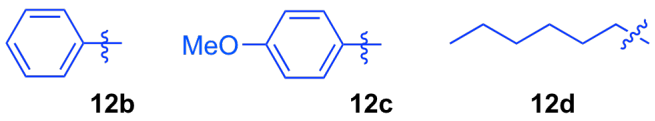

12b **12c** **12d**

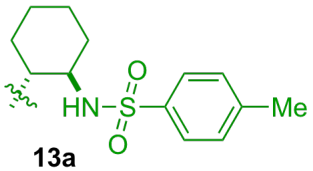

13a

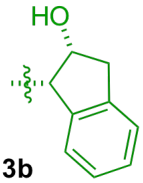

13b

Scheme S1. One-pot synthesis of squaramides **5**, **6** and **10**.

2. Expanded gelation tests

Table S1. Gelation tests with additional solvents.

entry	solvent[a]	phase[b]	optical appearance	lowest conc. (g L^{-1})[c]
1	dichloromethane	U		2
2	ethyl acetate	U		2
3	ethoxyethane	U		2
4	dibutylether	U		3
5	dimethylsulfoxid	sol	Yellowish solution	5
6	methylbenzene	U		2
7	trichloromethane	U		3
8	acetonitrile	PG	Partial gel with ungelled solvent and undissolved material	3
9	water	U		3
10	butan-2-ol	U		3
11	propan-2-ol	G + C	Weak gel with crystal growth after 1 h (collapses when turned upside-down)	6.5
12	glycerol	U		1
13	2-methylpentan-1-ol	G + U	Gel with undissolved compound. Clear solution obtained under "CGC"	"CGC" = 4.8
14	1,3-dichlorobenzene	G + U	Tendency to form gel-like material with undissolved solid remaining	4
15	2-(2-methoxyethoxy)ethanol	sol		5
16	2-furanmethanol	sol		5
17	2-(2-hydroxyethoxy)ethan-1-ol	PG	Tendency to form gel-like material	3.5
18	ethane-1,2-diol	G + U	Tendency to form gel-like material with undissolved material. Clear solution obtained under "CGC"	"CGC" = 4

[a] Solvent volume = 1 mL. [b] Abbreviations: G = gel; U = undissolved gelator; C = crystals, PG = partial gel. [c] Heating and ultrasound was applied in every case where unsolubility was observed.

3. Effect of gelator concentration on T_{gel}

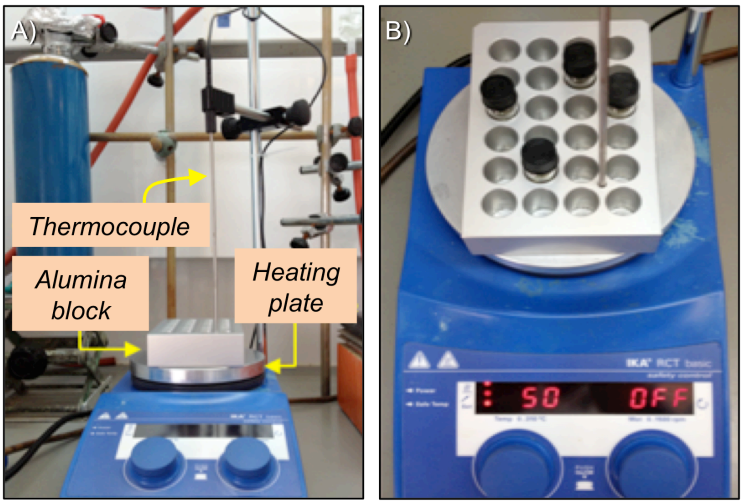

Figure S1. Thermoblock used for T_{gel} determinations. A) Front view of the set-up. B) Top view of the set-up during a typical experiment. The vials must fit smoothly inside the molds to ensure the optimal transmission of the heat flow.

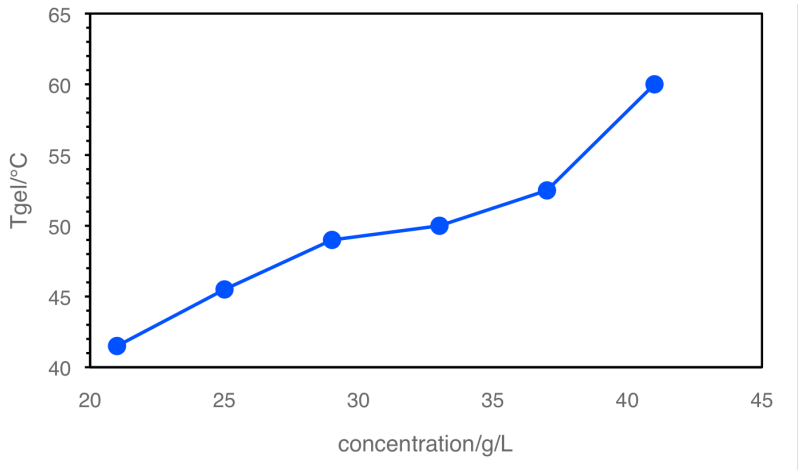

Figure S2. Evolution of T_{gel} with concentration of **1** in hexan-1-ol.

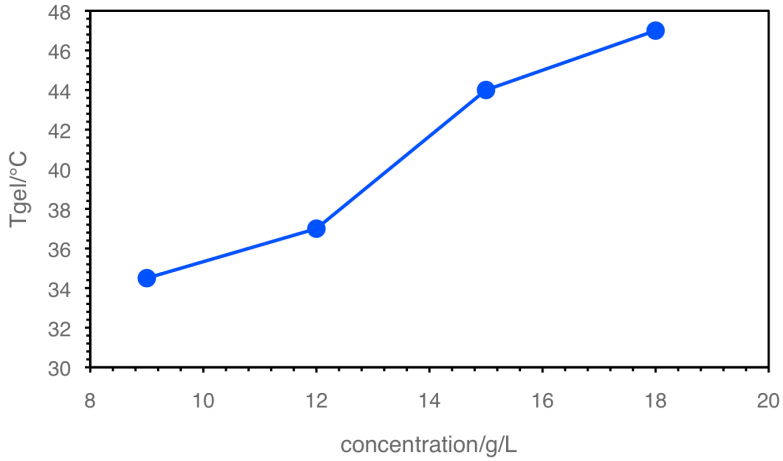

Figure S3. Evolution of T_{gel} with concentration of **1** in phenylmethanol.

4. ^{1}H-NMR and ^{13}C-NMR-APT spectra of new compounds

^{1}H-NMR and ^{13}C-NMR-APT spectra of squaramide **5**

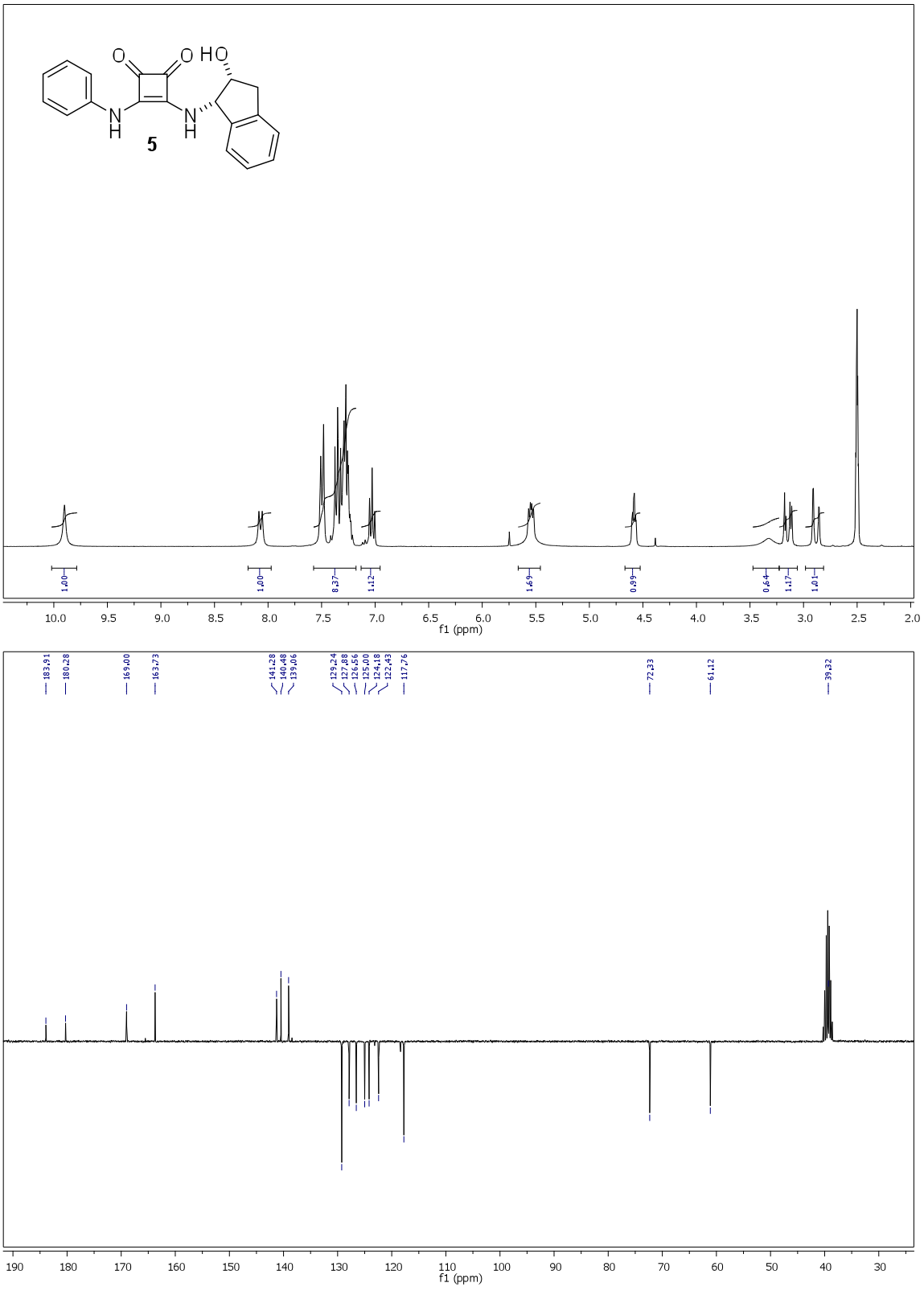

^{1}H-NMR and ^{13}C-NMR-APT spectra of squaramide **6**

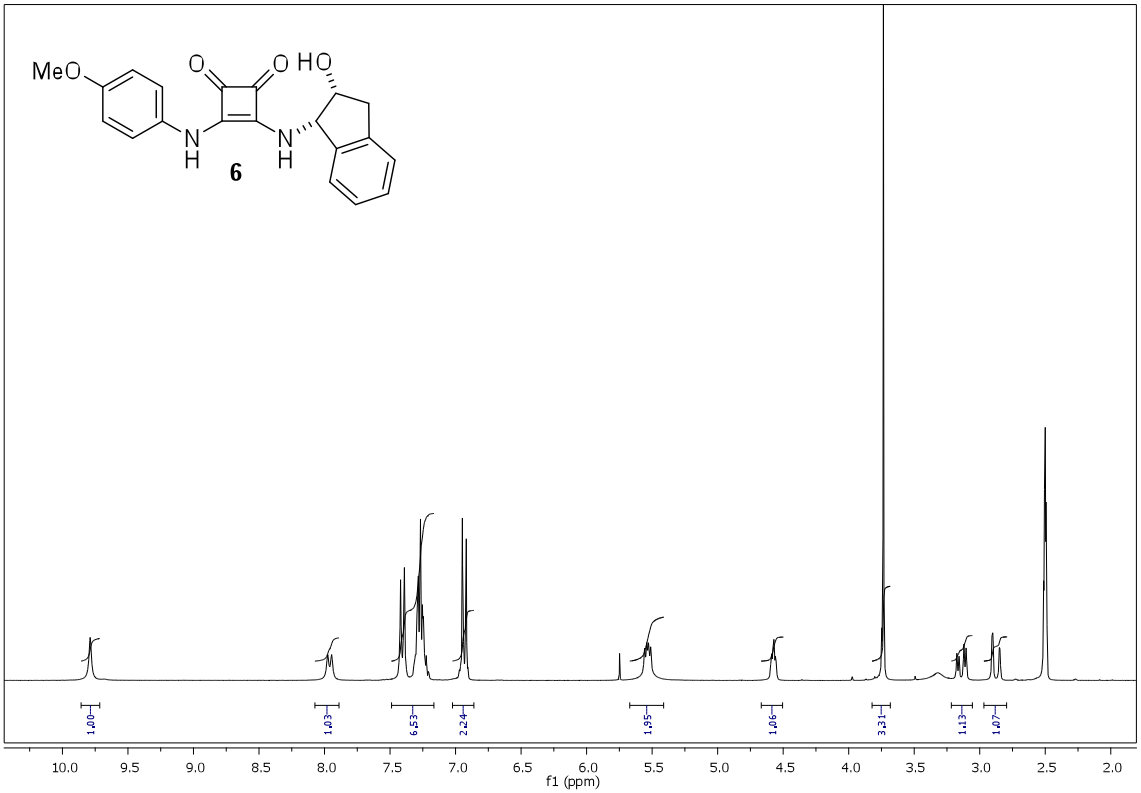

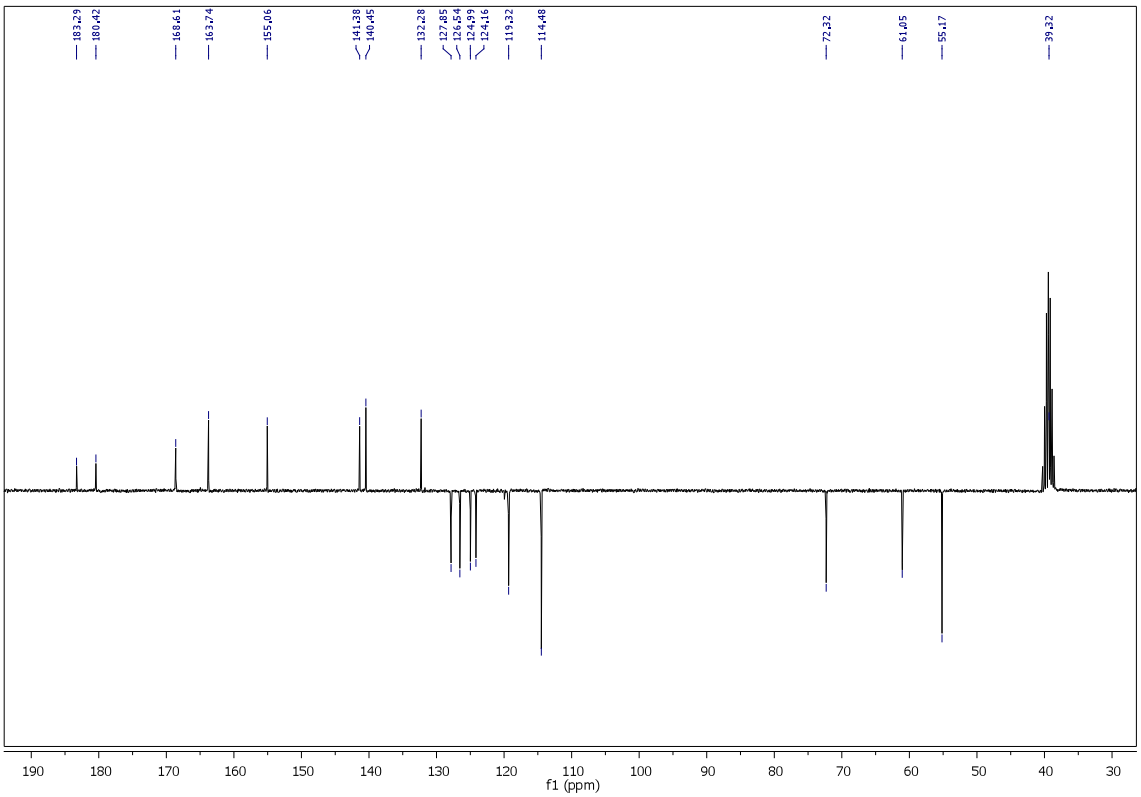

^{1}H-NMR and ^{13}C-NMR-APT spectra of squaramide **10**

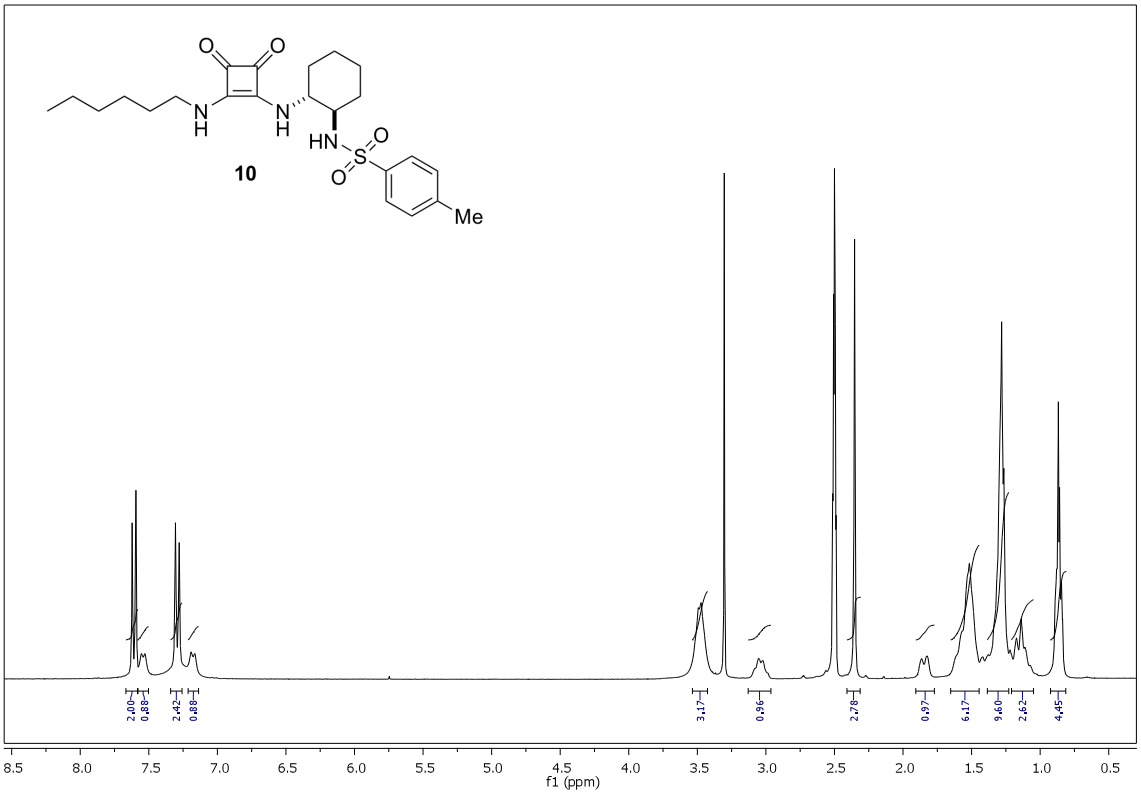

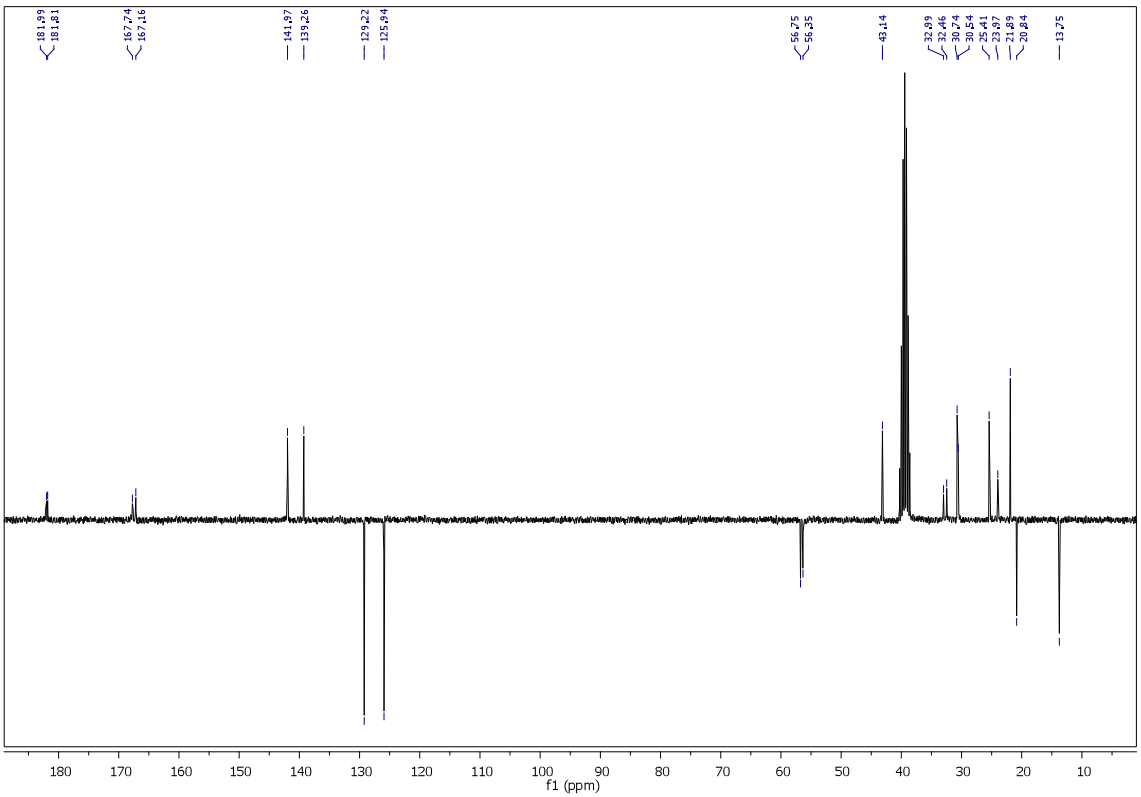

5. Representative FT-IR spectra

FT-IR spectrum of squaramide **5**

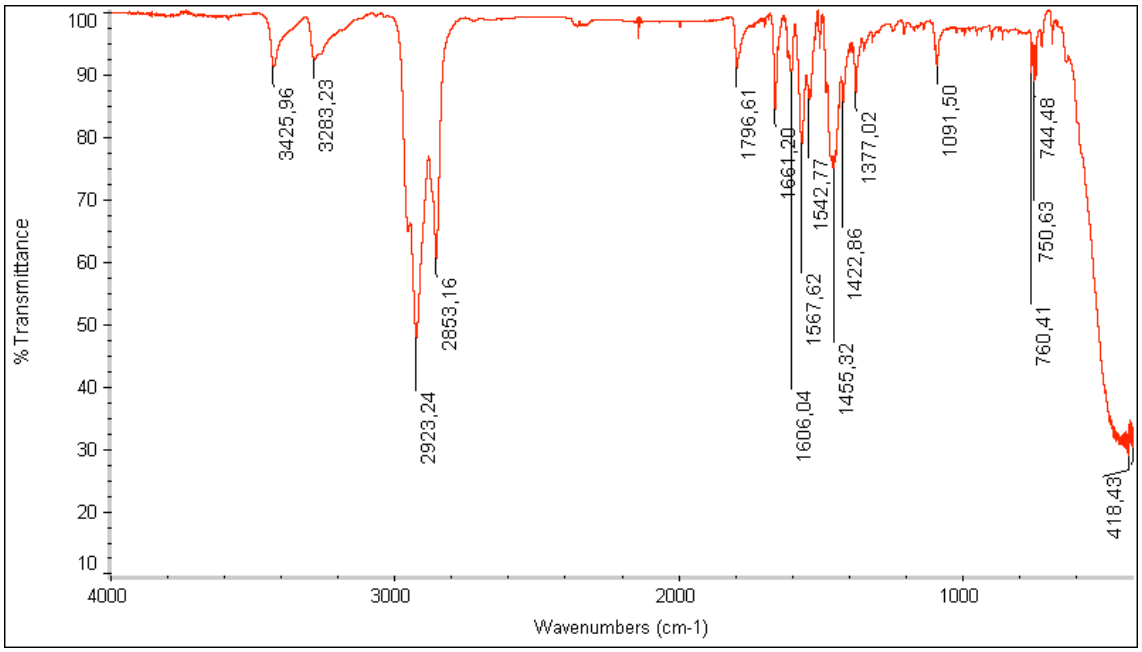

FT-IR spectrum of squaramide **6**

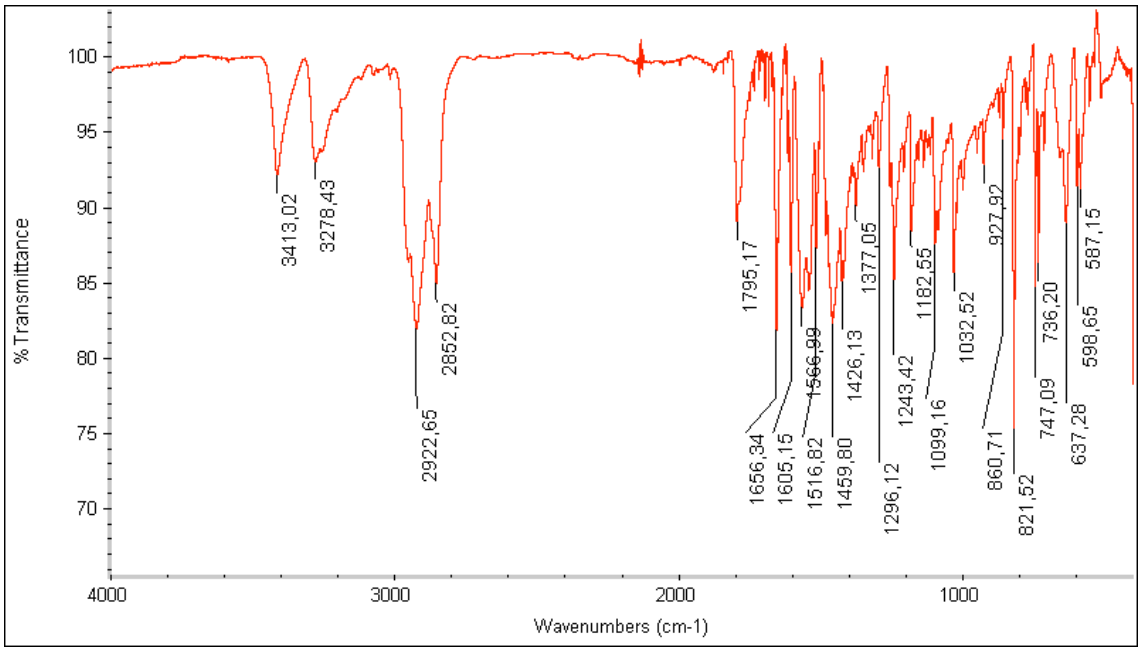

FT-IR spectrum of squaramide **10**

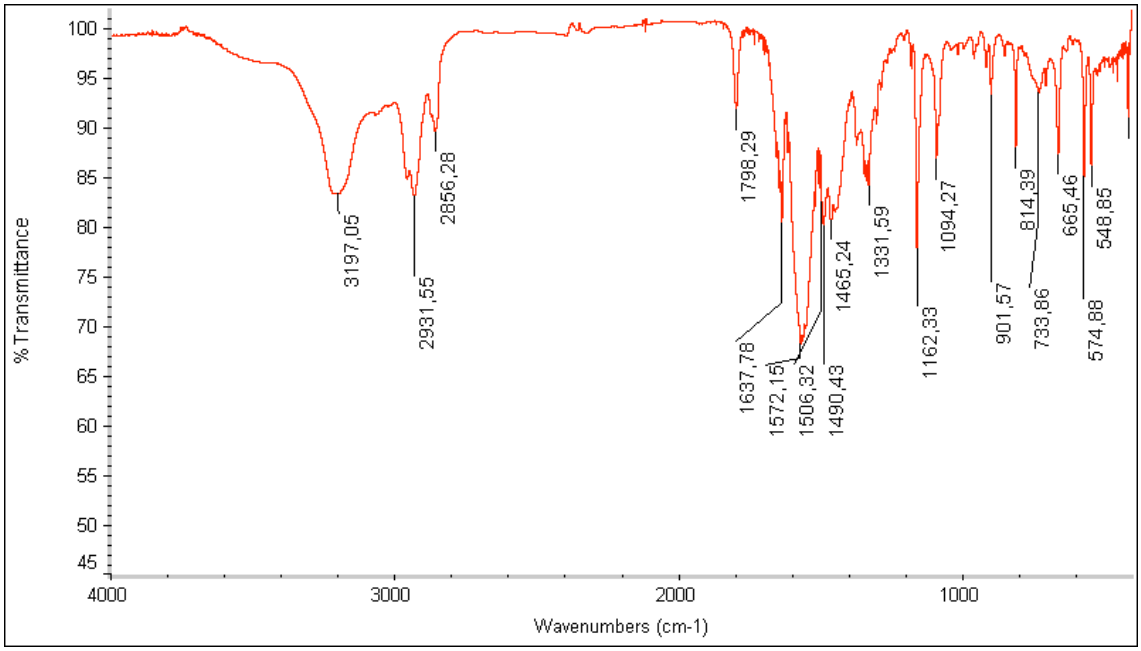

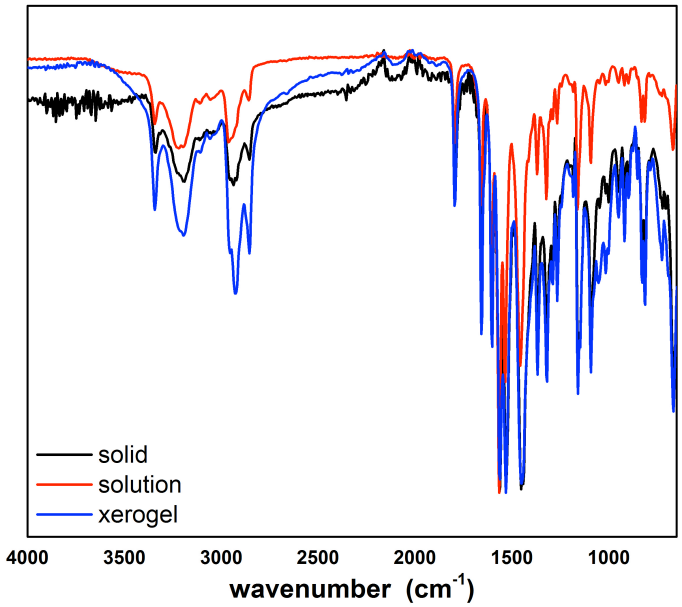

Figure S4. Representative FT-IR spectra of solid **1**, **1** in methanol solution and xerogel made from the corresponding organogel prepared using **1** in methanol.

6. Representative DSC

We thank Prof. Werner Kunz's group and PD R. Müller (Universität Regensburg) for giving us access to DSC and optical microscopes.

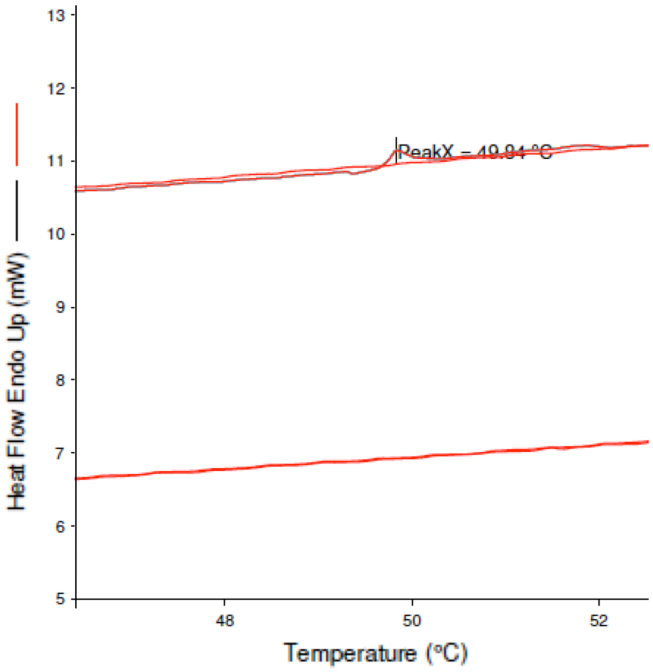

Figure S5. Representative DSC spectrum of two cycles corresponding to the gel made of **1** in methanol. Typically, gelator molecules assemble into fibers by a first-order process, which further self-assembles to form clusters and finally a 3D network. In general, the evolution of the cluster size is dominated by second-order thermal transitions.

7. Temperature-dependent NMR

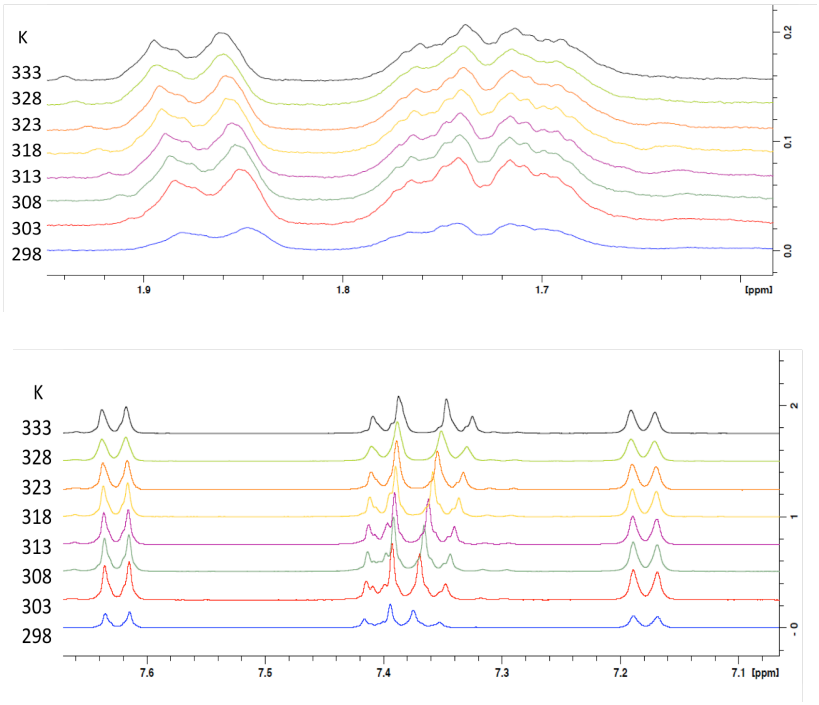

Figure S6. Selected regions of temperature-dependent ^{1}H-NMR spectra corresponding to the gel made of **1** in d_4-methanol.

8. Rheological measurements

Although the absolute values of the moduli can undergo significant variations under different rheometers and/or from batch to batch samples, the tan δ values (G''/G') were always reproducible. We thank Prof. Achim Göpferich's group (Universität Regensburg) for giving us access to the rheometer.

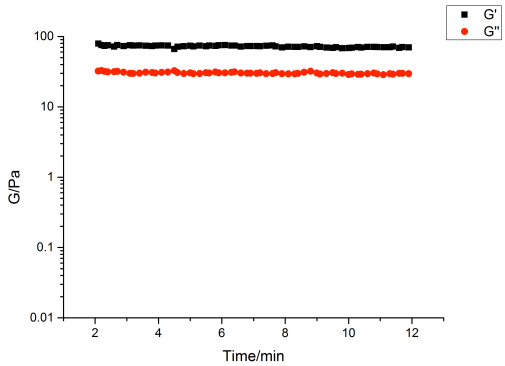

Phenylmethanol (DTS)

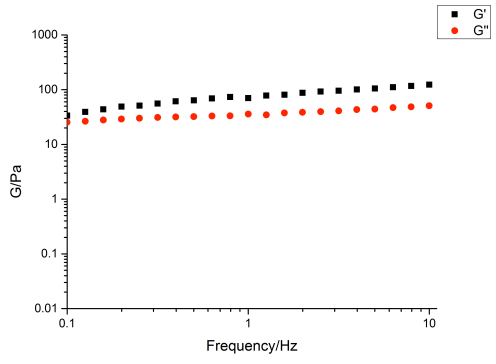

Phenylmethanol (DFS)

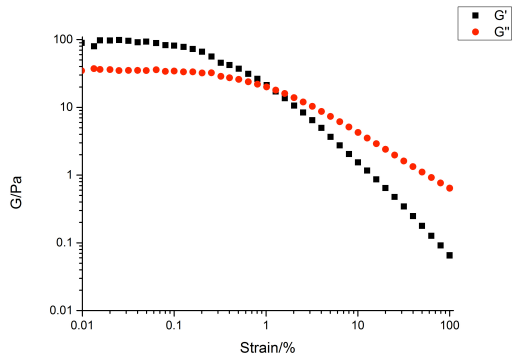

Phenylmethanol (DSS)

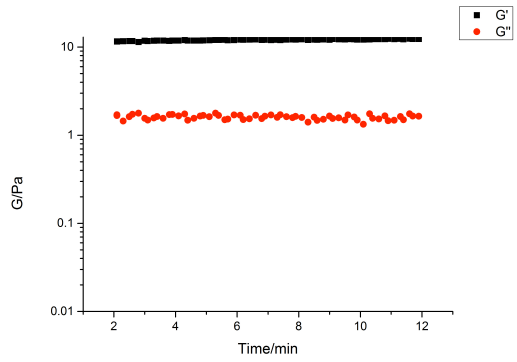

Hexan-1-ol (ultrasound) (DTS)

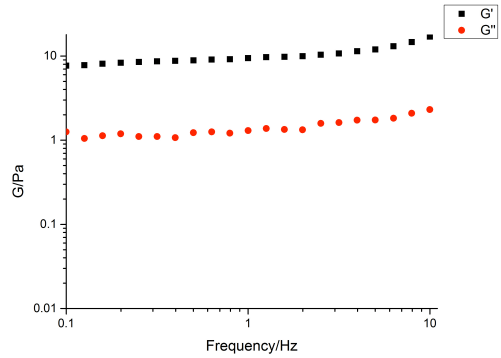

Hexan-1-ol (ultrasound) (DFS)

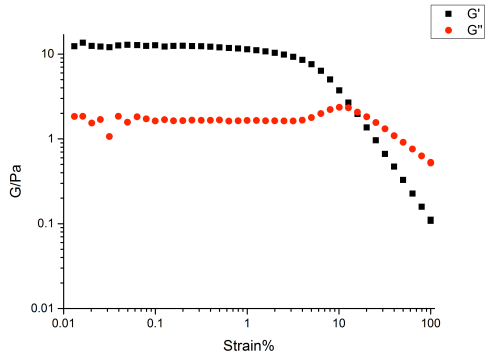

Hexan-1-ol (ultrasound) (DSS)

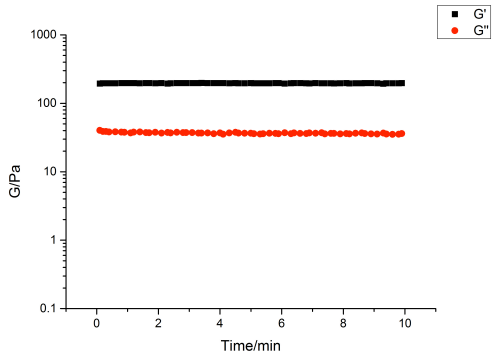

Hexan-1-ol (heating-cooling) (DTS)

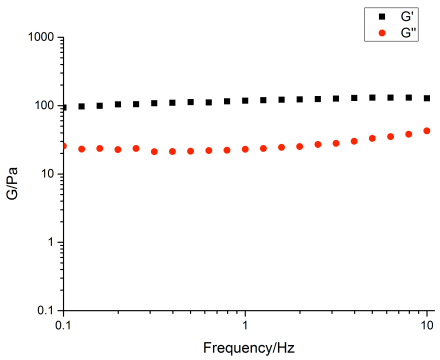

Hexan-1-ol (heating-cooling) (DFS)

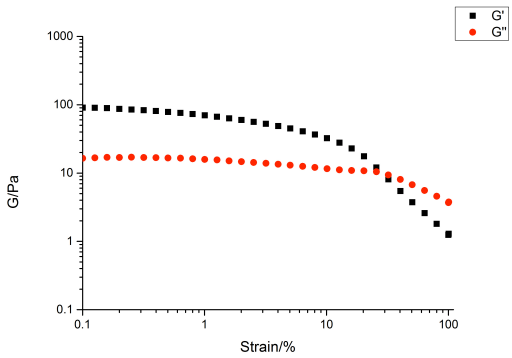

Hexan-1-ol (heating-cooling) (DSS)

Figure S7. Oscillatory rheological experiments (DSS, DFS, DTS) of model gels prepared as described in Table 1 in the main paper.

9. Additional FESEM, TEM and AFM images

We would like to acknowledge the use of Servicio General de Apoyo a la Investigación-SAI, Universidad de Zaragoza, for FESEM and TEM imaging, as well as the Laboratorio de Microscopías Avanzadas at Instituto de Nanociencia de Aragón, Universidad de Zaragoza, for AFM measurements.

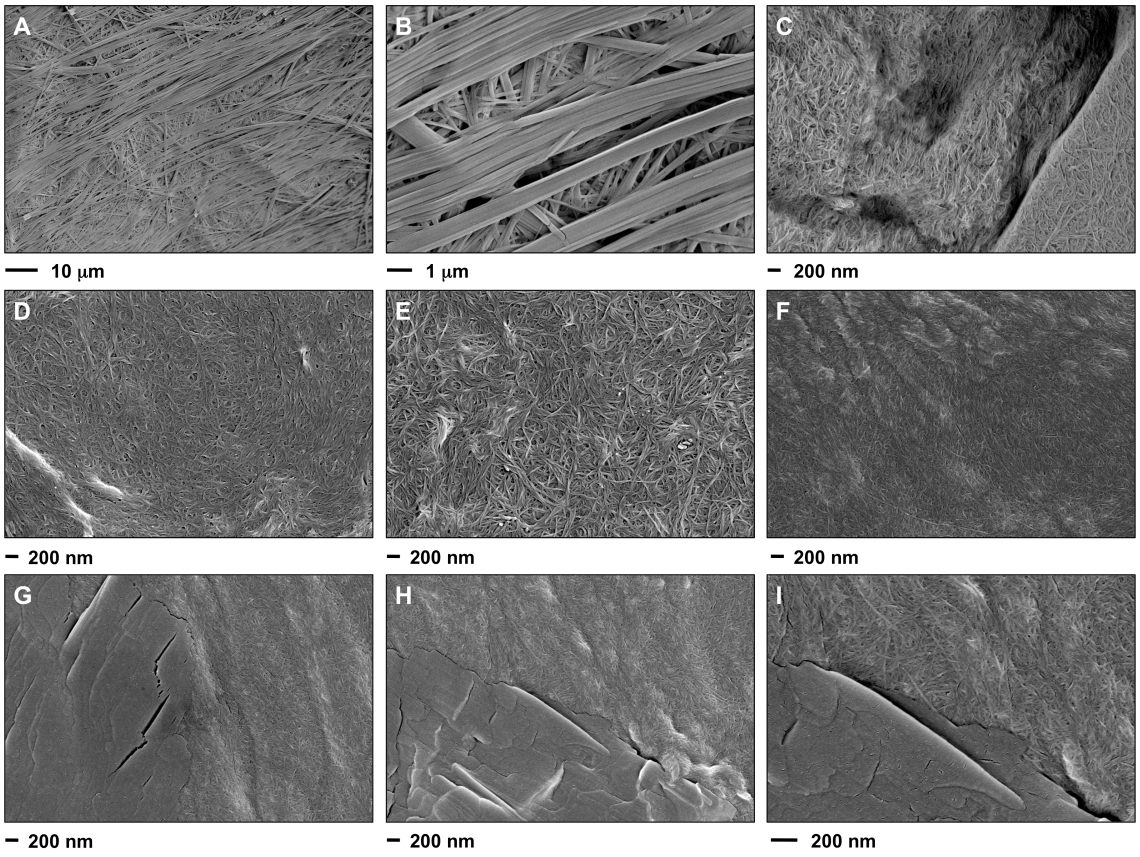

Figure S8. Additional FESEM images of the xerogels obtained from the corresponding gels. A-B) phenylmethanol (heating-cooling). C) hexan-1-ol (heating-cooling). D-E) hexan-1-ol (heating-ultrasound). F-I) methanol (heating-cooling).

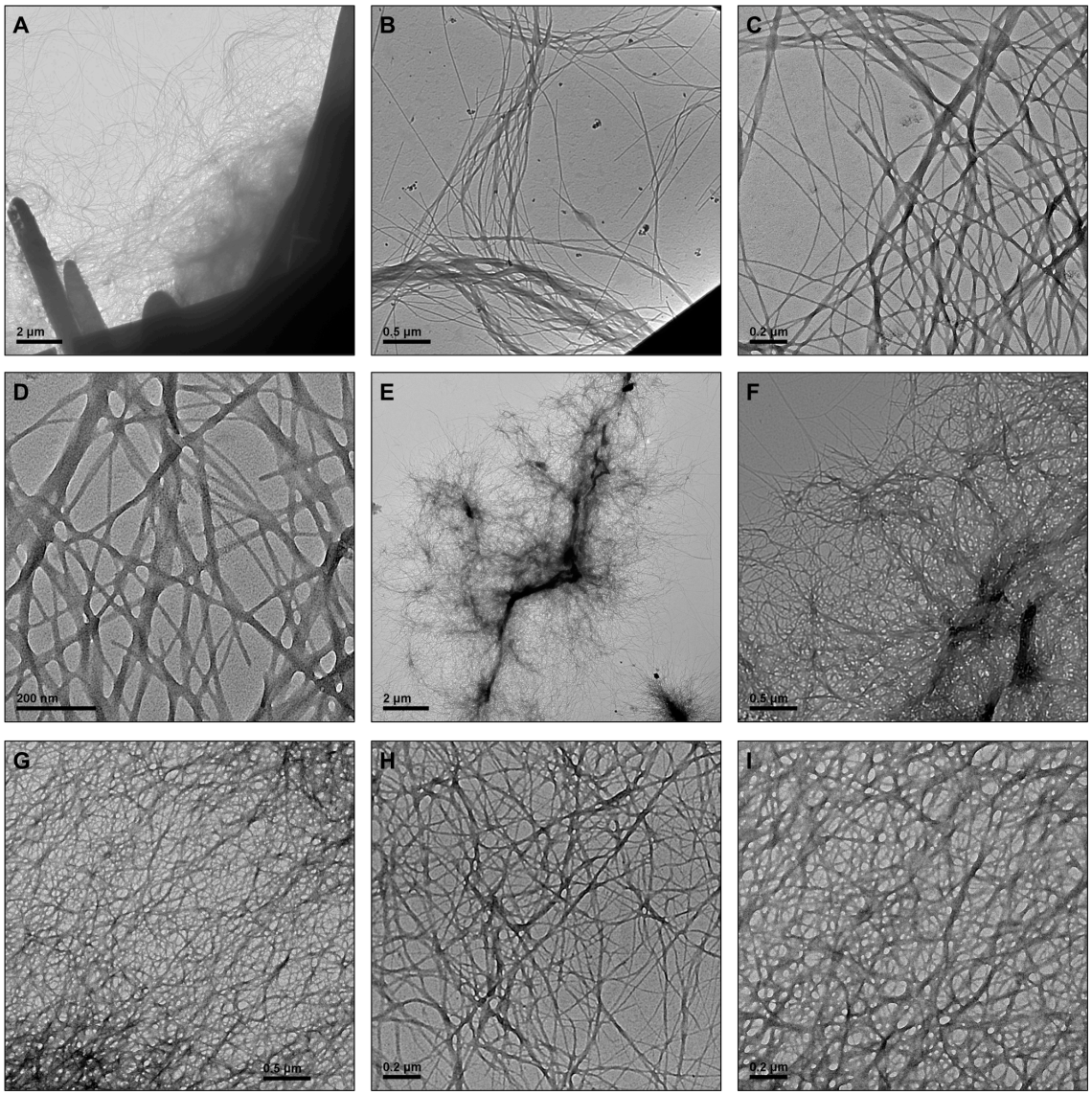

Figure S9. Additional TEM images of the xerogels obtained from the corresponding gels prepared at the CGC. A-D) hexan-1-ol (heating-cooling). E-I) methanol (heating-cooling).

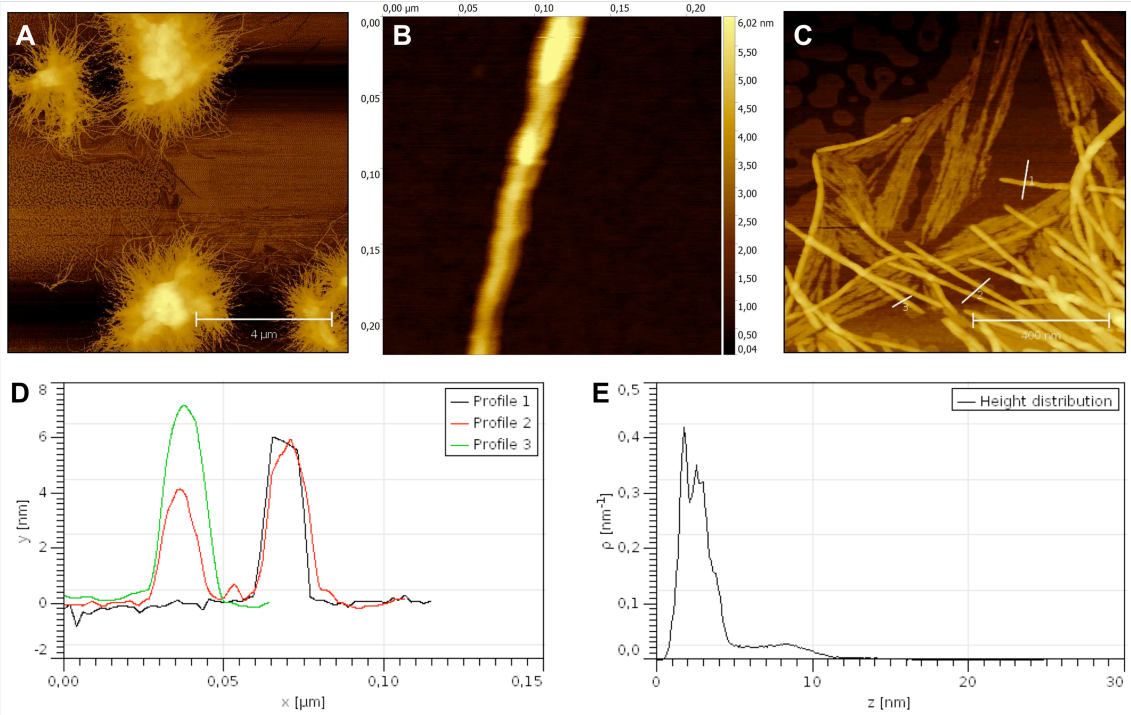

Figure S10. A-C) Additional AFM images of the gel prepared in methanol at CGC. D) Profile of the fiber unit. E) Histogram. Scale bars: A) 4 µm; C) 400 nm.

10. Additional optical microscopy images

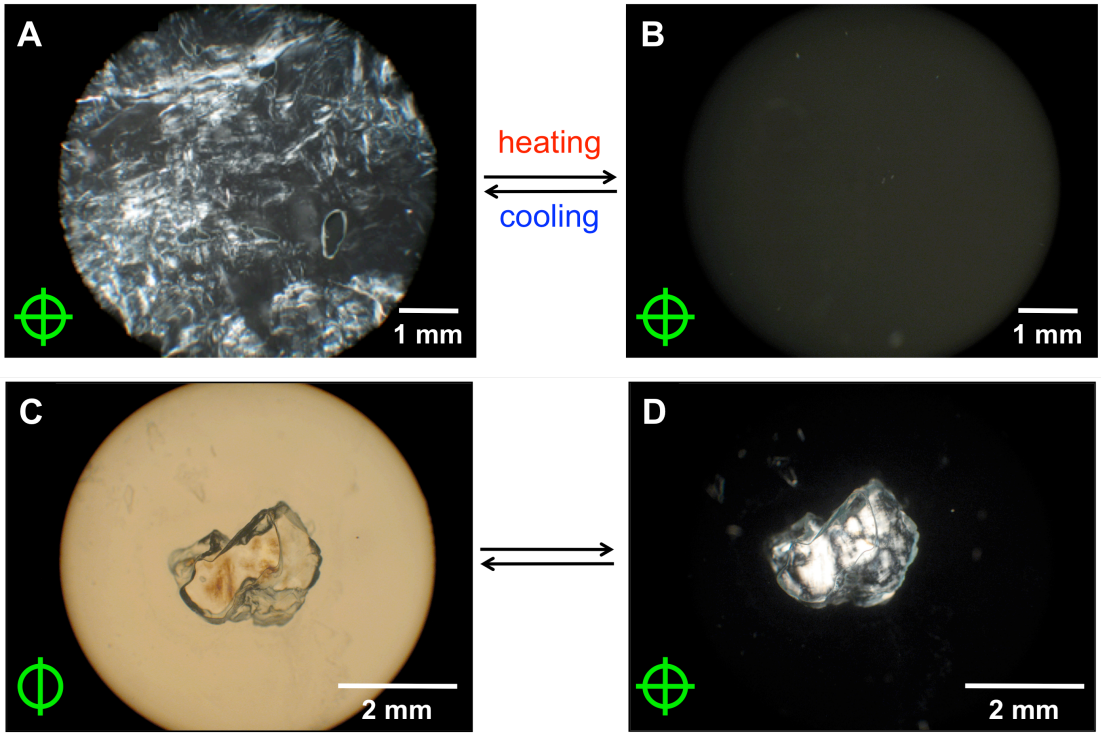

Figure S11. A-B) Polarized light (90º) microscope images of A) alcogel made of **1** in methanol at CGC (c = 7 g L^{-1}) and B) solution upon *gel*-to-*sol* thermal transition. B-C) Bulk gel made of **1** in methanol (c = 15 g L^{-1}) (A) without and (B) with crossed polarizers.

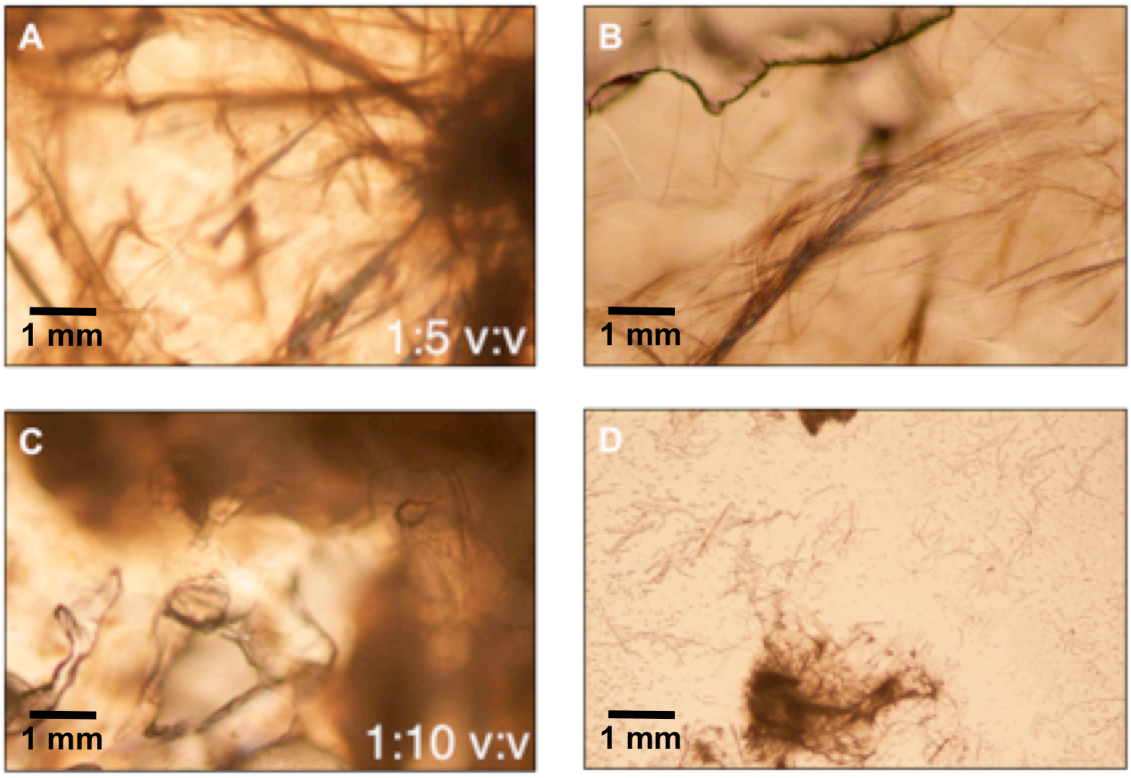

Figure S14. Optical microscope images of precipitated compound **1** in methanol-water mixture: A-B) 1:5 v:v water/methanol (nearly complete gelation, solvent overlap ca. 10%). C-D) 1:10 v:v water/methanol (nearly complete gelation, solvent overlap ca. 7%).

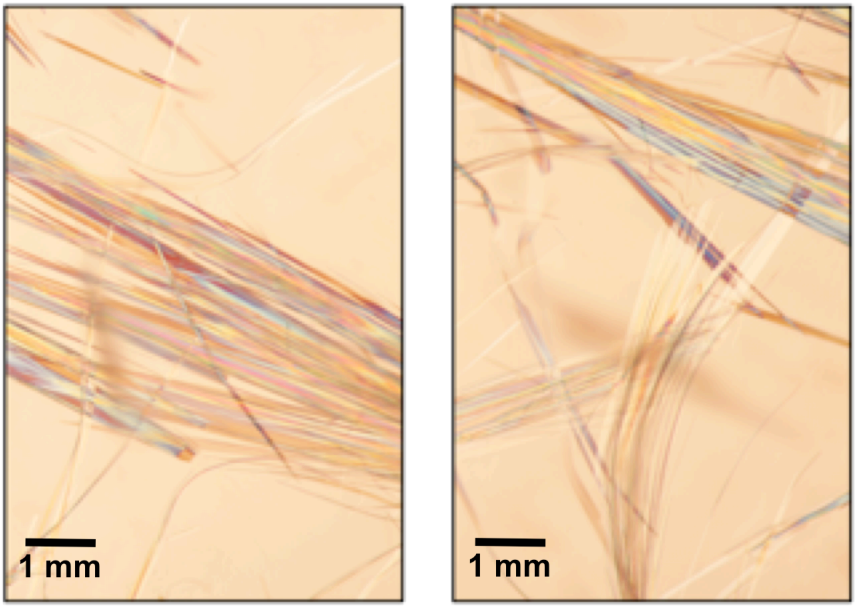

Figure S15. Crystals observed inside the gel made of **1** in 2-methylbutan-1-ol at CGC (c = 4.7 g L^{-1}) by heating-cooling.

11. PXRD

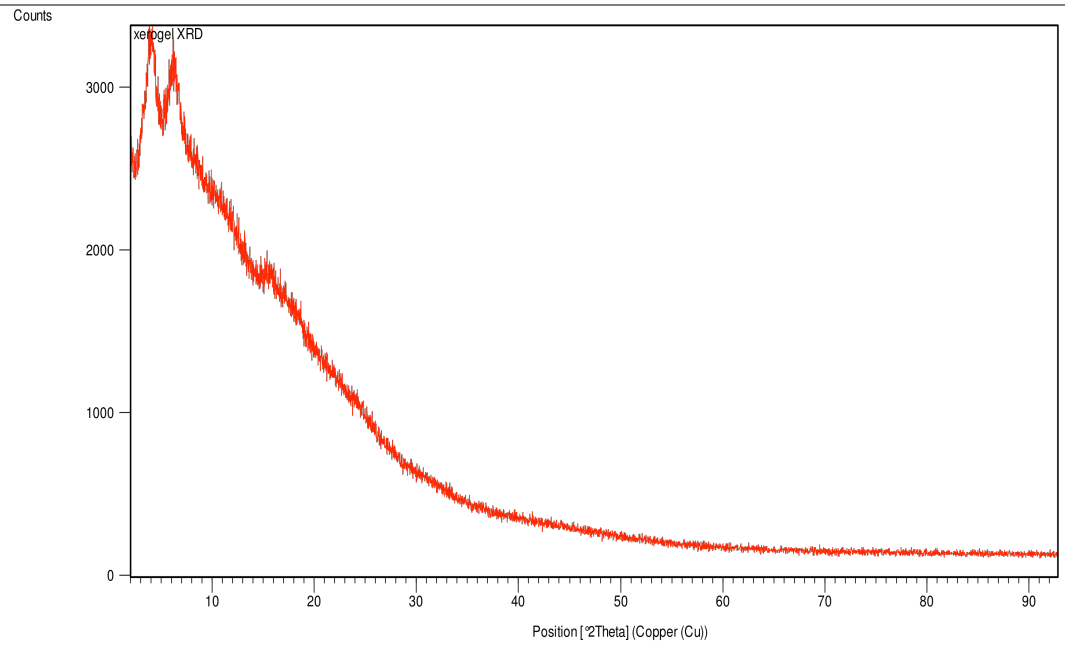

PXRD of the xerogel obtained from the corresponding gel made of **1** in methanol at CGC (c = 7 g L^{-1}).

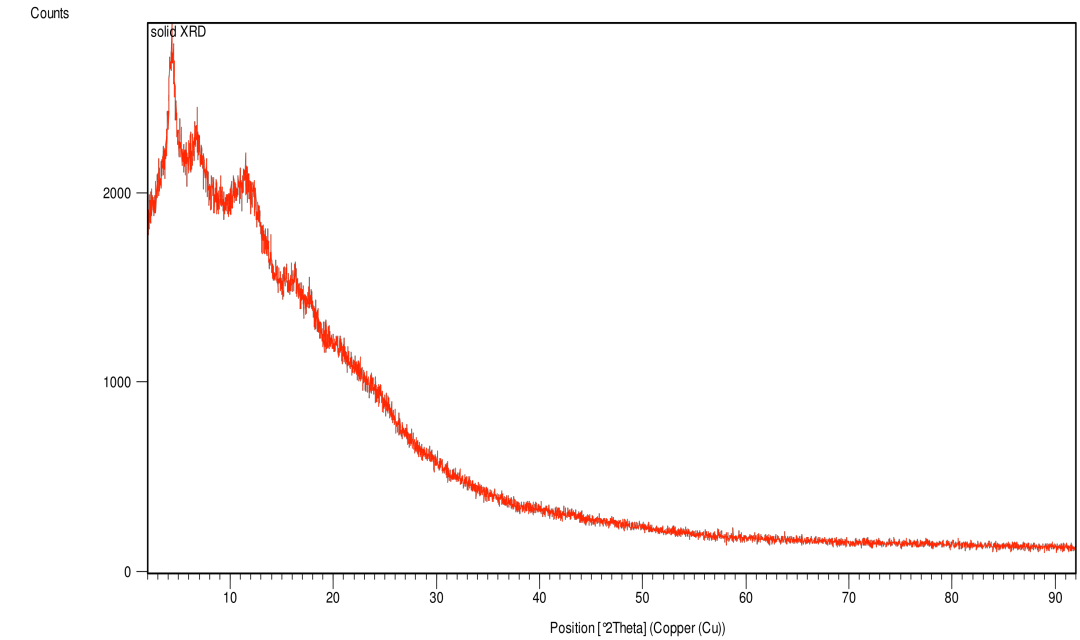

PXRD of the squaramide **1**.

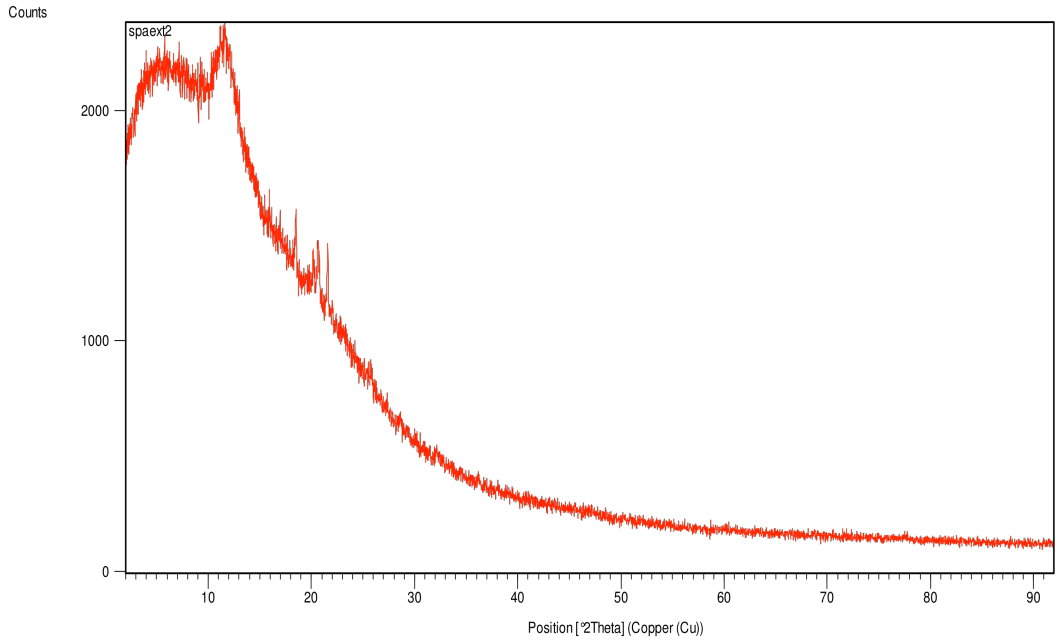

PXRD of the squaramide **2**.

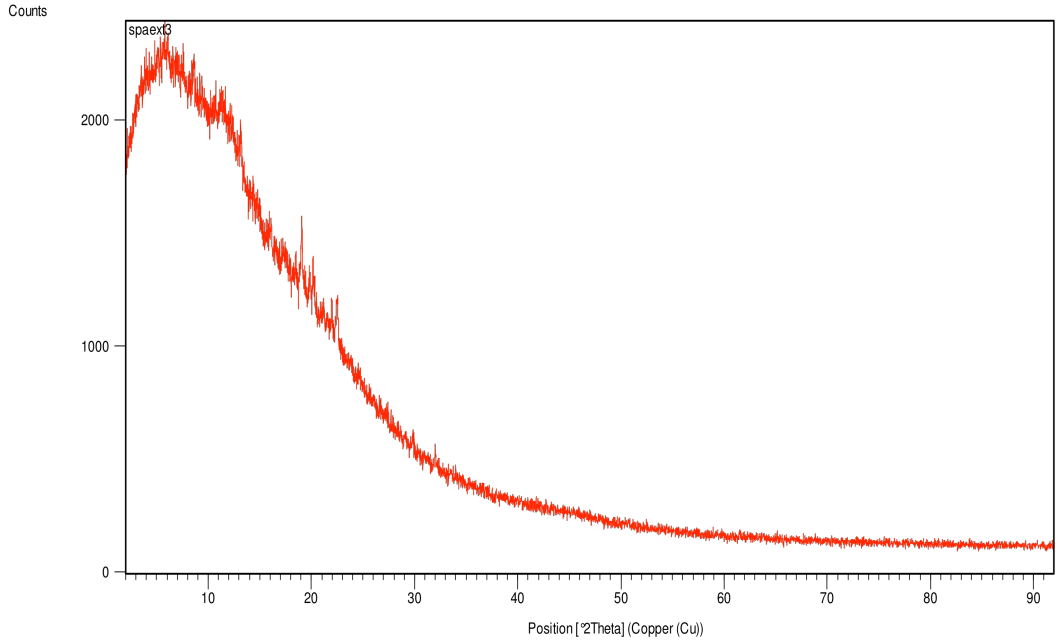

PXRD of the squaramide **3**.

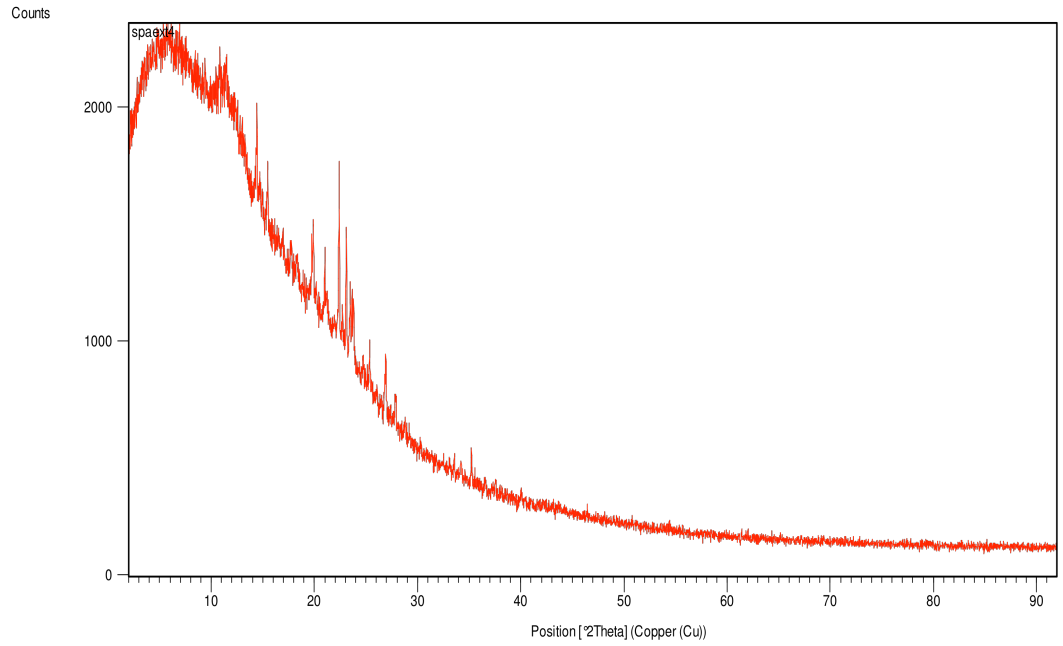

PXRD of the squaramide **4**.

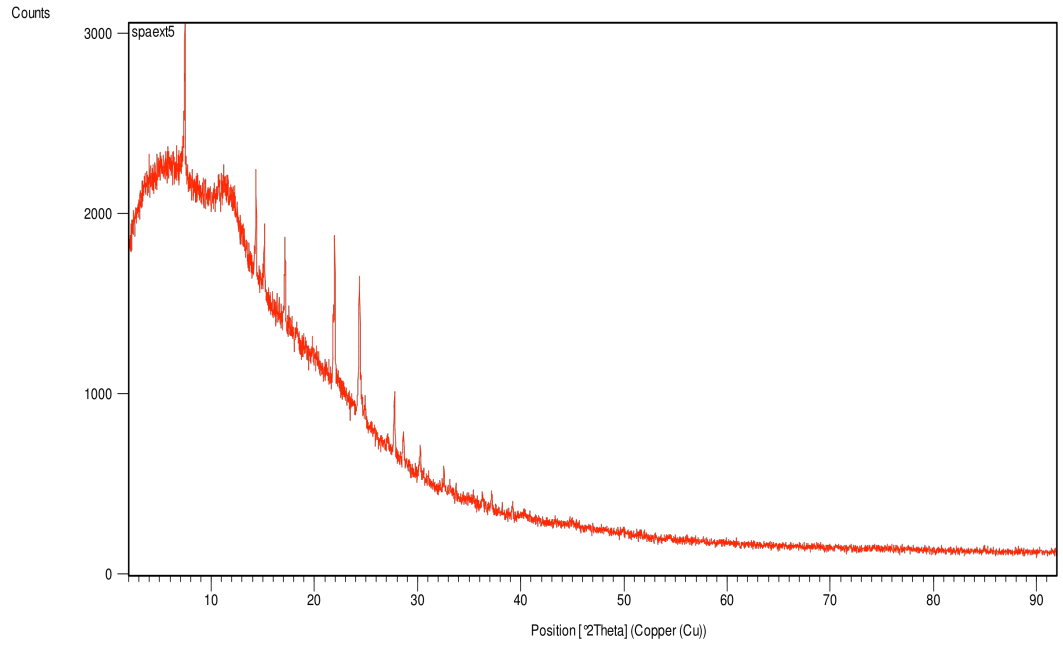

PXRD of the squaramide **5**.

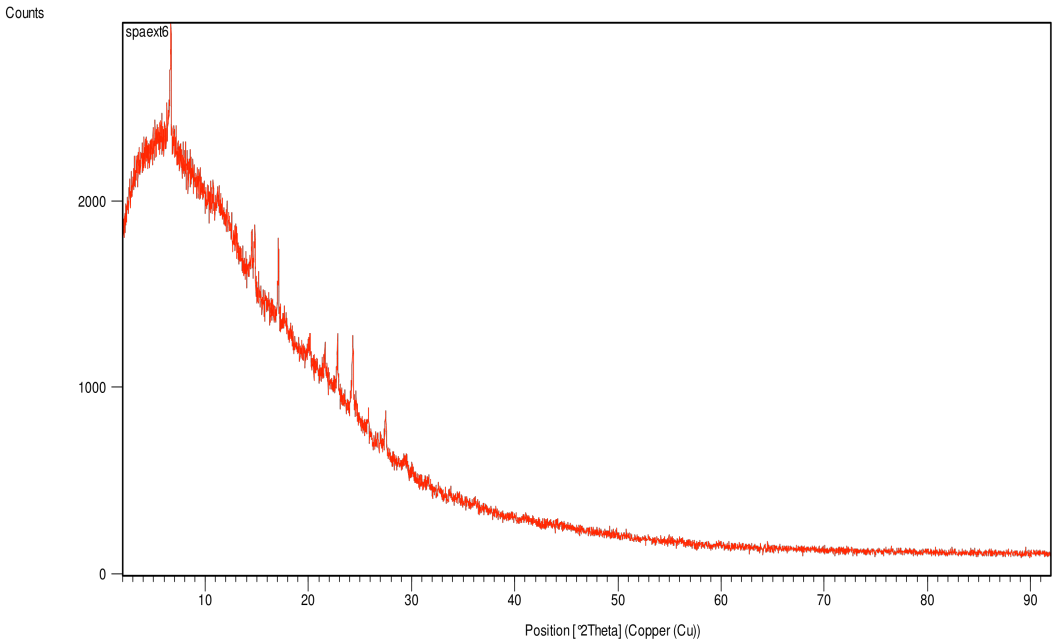

PXRD of the squaramide **6**.

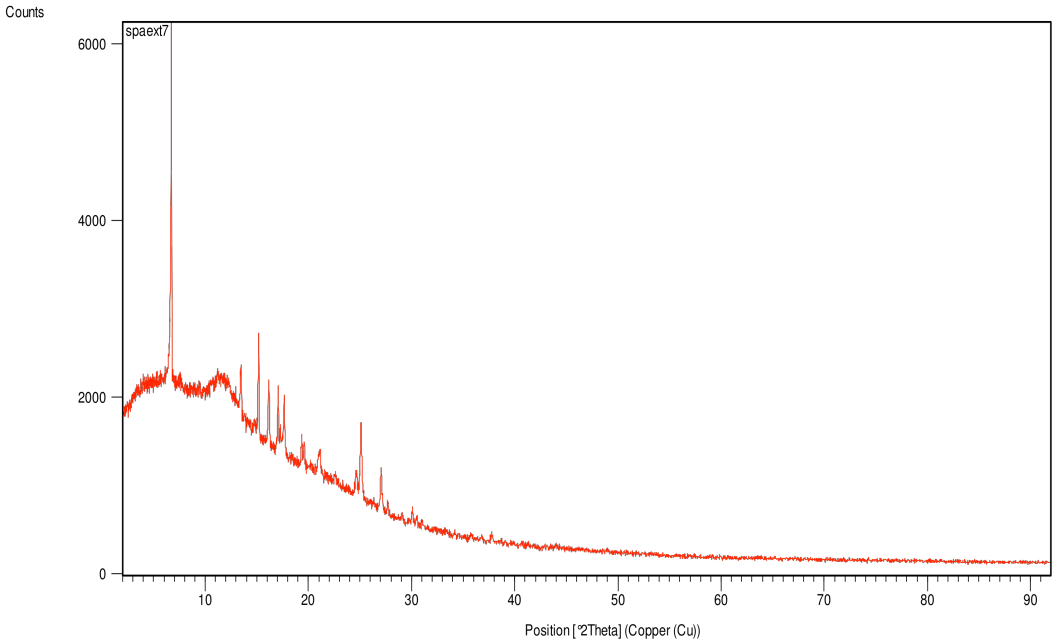

PXRD of the squaramide **7**.

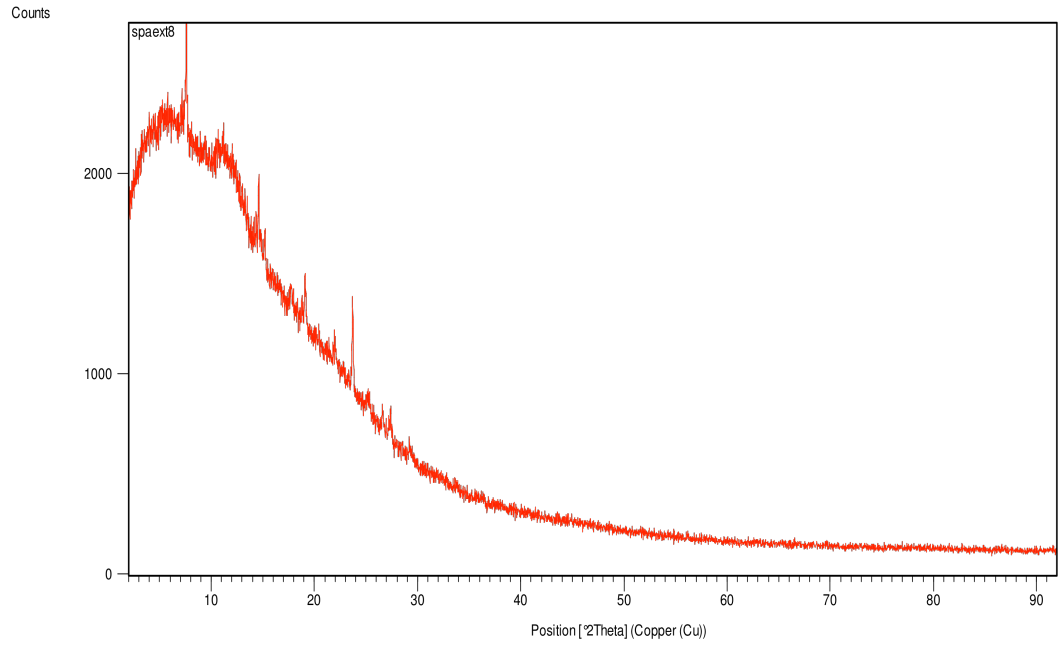

PXRD of the squaramide **8**.

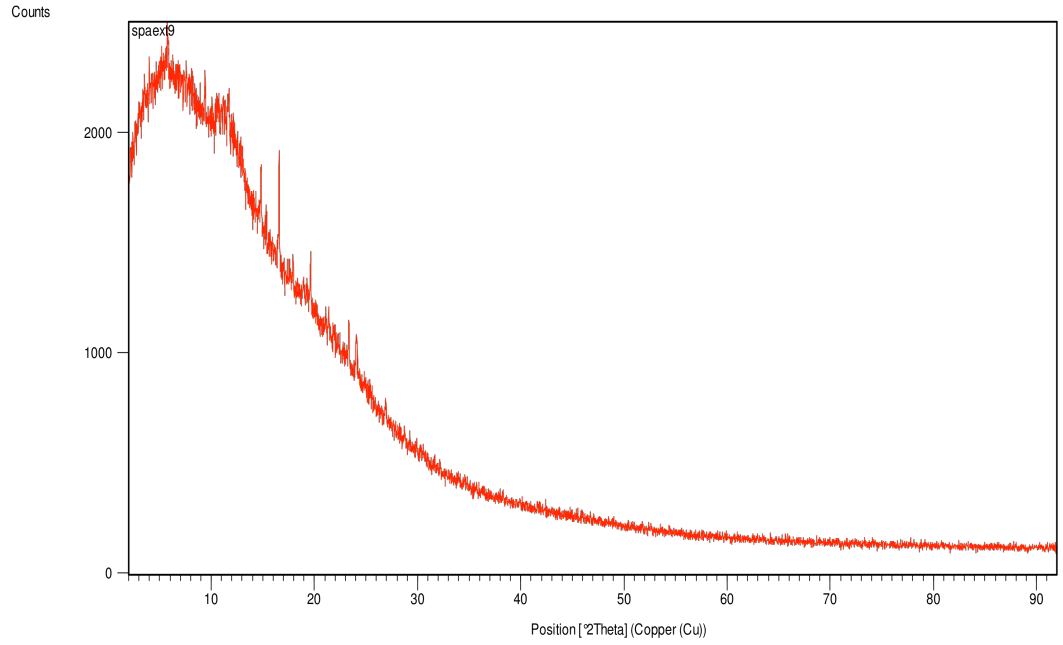

PXRD of the squaramide **9**.

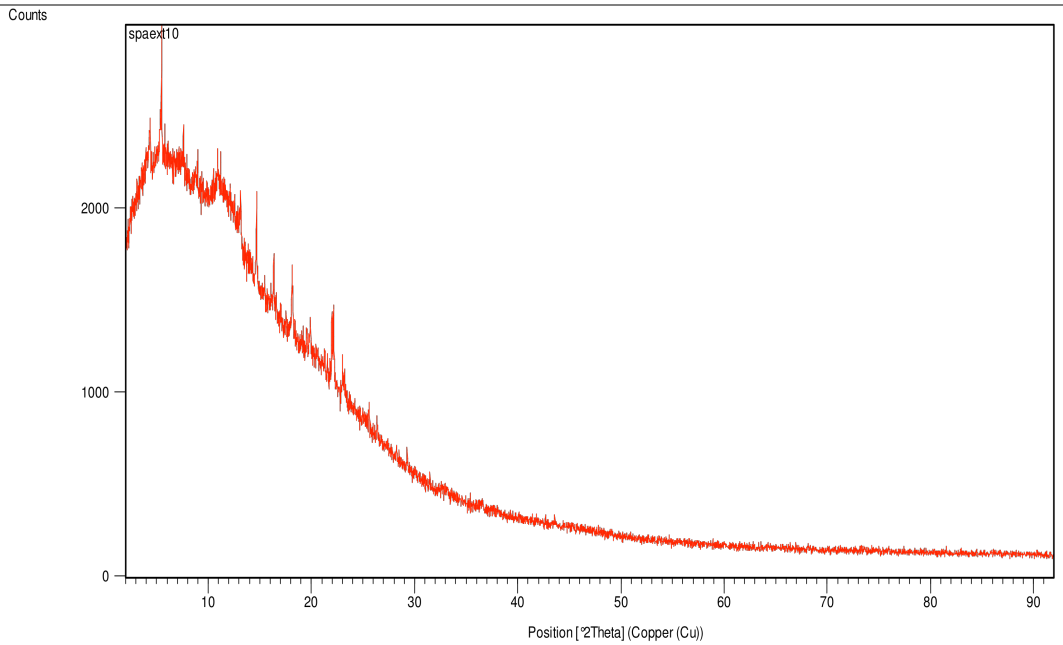

PXRD of the squaramide **10**.

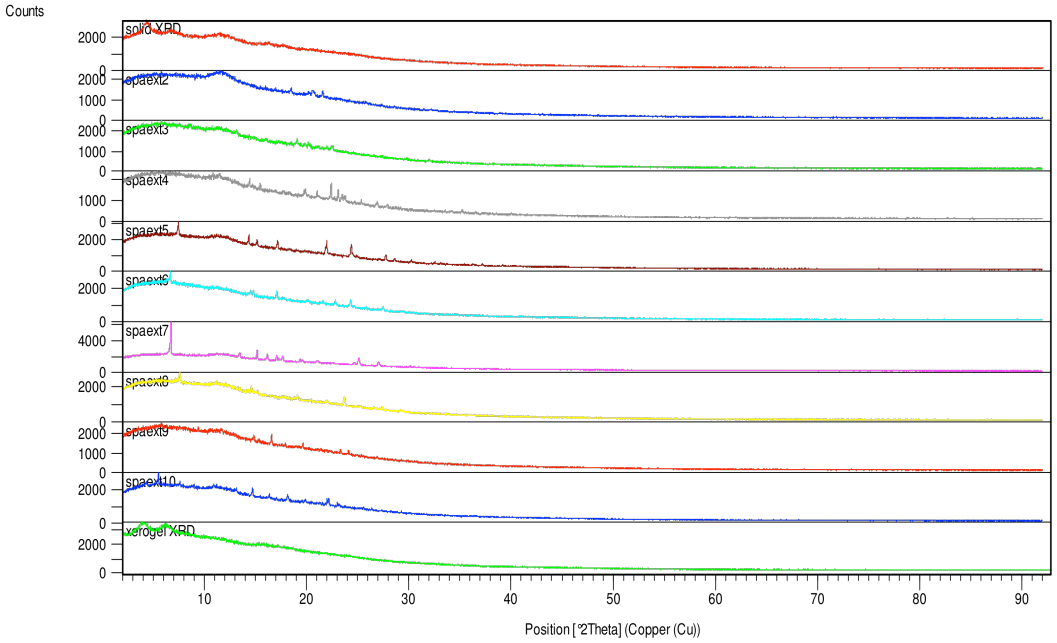

Compilation of above PXRD spectra. From top to down: xerogel made of **1**, squaramide **2**, squaramide **3**, squaramide **4**, squaramide **5**, squaramide **6**, squaramide**7**, squaramide **8**, squaramide **9**, squaramide **10**, squaramide **1**.

Figure S16. PXRD spectra of gelator (as xerogel and as synthesized solid gelator) and non-gelator squaramides. 2θ (Bragg's angle) range $2º \leq 2\theta \leq 90º$.

Table S2. Major peaks of the spectra shown in Figure S16 and the corresponding lattice spacings calculated from Bragg's law ($n\lambda = 2d\sin\theta$).

Sample	2θ (º)	*d* (Å) (respectively)
Xerogel made of **1**	3.96, 6.18, 15.70	22.28, 14.30, 5.64
Squaramide **1**	4.41, 6.71, 11.51, 16.35, 17.90	20.00, 13.16, 7.68, 5.42, 4.95
Squaramide **2**	11.69, 18.50, 20.64, 21.58	7.56, 4.78, 4.30, 4.12
Squaramide **3**	19.06, 20.22, 22.52	4.65, 4.39, 3.94
Squaramide **4**	11.55, 14.43, 15.46, 19.89, 21.01, 22.41, 23.11, 23.47, 23.74, 25.36, 26.92, 27.89, 35.23	7.65, 6.13, 5.73, 4.46, 4.23, 3.96, 3.85, 3.79, 3.74, 3.51, 3.31, 3.20, 2.55
Squaramide **5**	7.47, 11.45, 14.35, 15.17, 17.17, 21.98, 24.39, 27.76, 28.62, 30.25, 32.56, 37.17	11.83, 7.23, 6.17, 5.84, 5.16, 4.04, 3.65, 3.21, 3.12, 2.95, 2.75, 2.42
Squaramide **6**	6.69, 14.52, 14.81, 17.10, 20.08, 21.59, 22.81, 24.32, 25.81, 27.50, 29.40	13.21, 6.09, 5.98, 5.18, 4.42, 4.11, 3.89, 3.66, 3.49, 3.24, 3.04
Squaramide **7**	6.73, 11.81, 13.49, 15.18, 16.16, 17.08, 17.68, 19.37, 19.62, 20.20, 21.13, 22.59, 24.63, 25.11, 27.06, 27.70, 29.07, 30.10, 30.50, 37.80	13.12, 7.47, 6.56, 5.83, 5.48, 5.19, 5.01, 4.58, 4.52, 4.39, 4.20, 3.93, 3.61, 3.54, 3.29, 3.22, 3.07, 2.97, 2.92, 2.38
Squaramide **8**	7.62, 11.32, 14.59, 19.11, 22.00, 23.72, 25.20, 26.63, 27.37, 29.31	11.59, 7.81, 6.07, 4.64, 4.04, 3.75, 3.53, 3.34, 3.26, 3.05
Squaramide **9**	5.73, 11.68, 14.84, 16.59, 19.63, 23.34, 24.08	15.40, 7.57, 5.96, 5.34, 4.52, 3.81, 3.69
Squaramide **10**	4.36, 5.50, 7.61, 10.99, 13.11, 14.71, 16.34, 18.16, 19.80, 22.00, 22.16, 23.11	20.24, 16.04, 11.61, 8.04, 6.75, 6.02, 5.42, 4.88, 4.48, 4.04, 4.00, 3.85

13. UV-vis

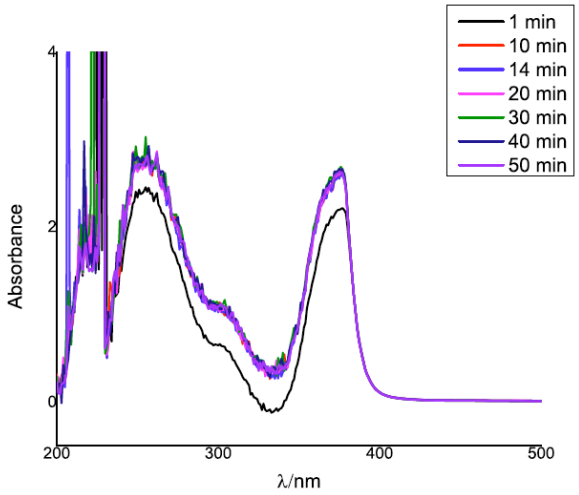

Figure S17. Evolution of the UV-vis spectra during the *sol*-to-*gel* transition of the sample containing **1** in methanol at a concentration of 10 g L^{-1}.

13. Additional photographs of materials prepared under different conditions

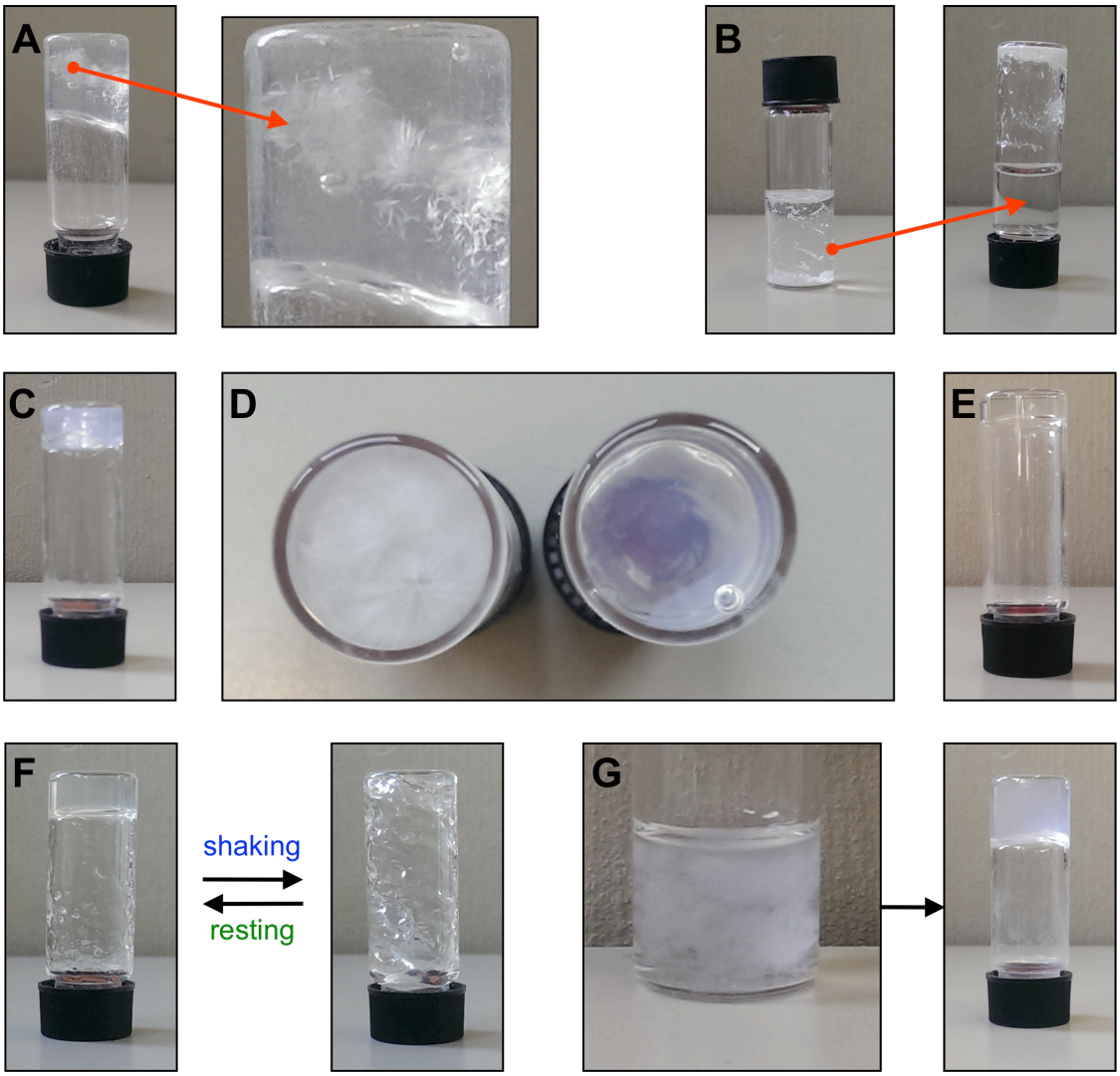

Figure S18. A) Crystal growth within 18 h inside the gel made of **1** in ethanol (c = 5.5 g L^{-1}) via heating-ultrasound. B) Gelation test of **1** in acetonitrile led to precipitation of the gelator. C) Gel obtained in acetone at c = 7.3 g L^{-1} via heating-ultrasound. D) Mixture of **1** in propan-1-ol (c = 5.5 g L^{-1}) after heating-cooling (*left vial*) and heating-ultrasound (*right vial*). Crystallization within the bulk gel is evident in the case of heating-cooling. E) Stable gel made of **1** in butan-1-ol (c = 10.5 g L^{-1}). F) Macroscopic thixotropic behavior of the gel made of **1** in butan-1-ol at CGC. Complete recovery of the destroyed gel phase took ca. 2 h. G) Milky aspect of the mixture of **1** in 2-methylpropan-2-ol (c = 3.1 g L^{-1}) after heating. Heating-ultasound was applied to obtain a stable gel after 51 h.

14. Quantum mechanical calculations

14.1. Representation of the two most stable complexes obtained for **7**

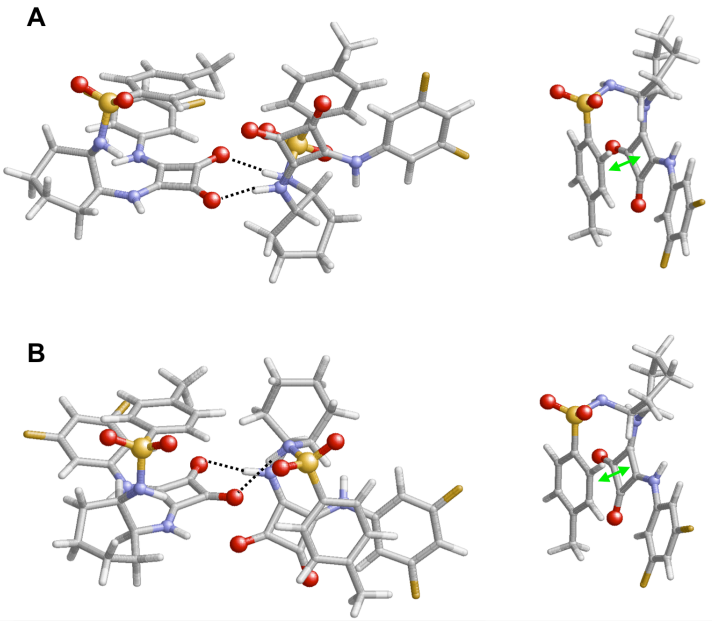

Figure S19. Representation of the two most stable complexes obtained for **7**: A) $\Delta E_i = -19.7$ kcal mol^{-1} and B) $\Delta E_i = -19.2$ kcal mol^{-1}. Intermolecular (*left*) and intramolecular (*right*) interactions are displayed for the complex and a single molecule of the complex, respectively. Hydrogen bonds are represented by black dashed lines and intramolecular π···π stacking interactions by green double arrows.

14.2. Representation of the two most stable complexes obtained for **10**

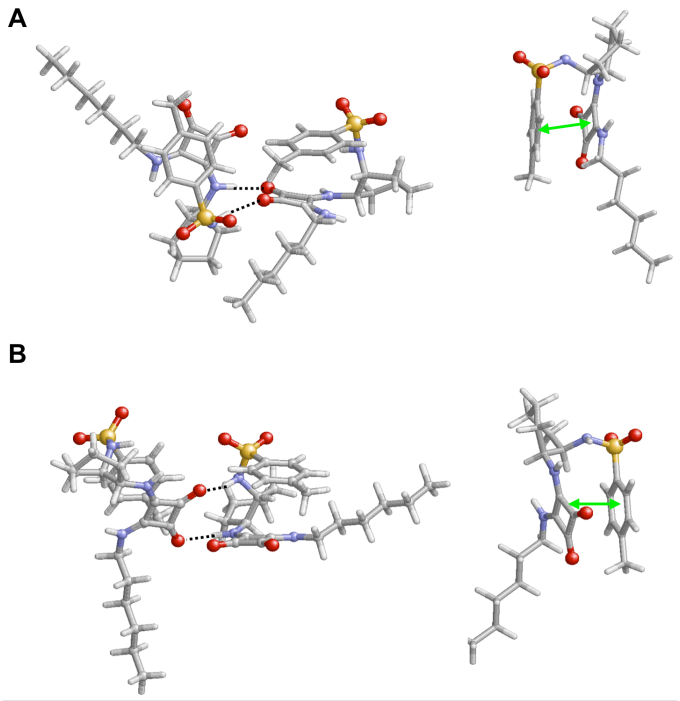

Figure S20. Representation of the two most stable complexes obtained for **10**: A) $\Delta E_i = -20.5$ kcal mol^{-1} and B) $\Delta E_i = -18.8$ kcal mol^{-1}. Intermolecular (*left*) and intramolecular (*right*) interactions are displayed for the complex and a single molecule of the complex, respectively. Hydrogen bonds are represented by black dashed lines and intramolecular π···π stacking interactions by green double arrows.

14.3. Representation of the two most stable complexes obtained for **8**

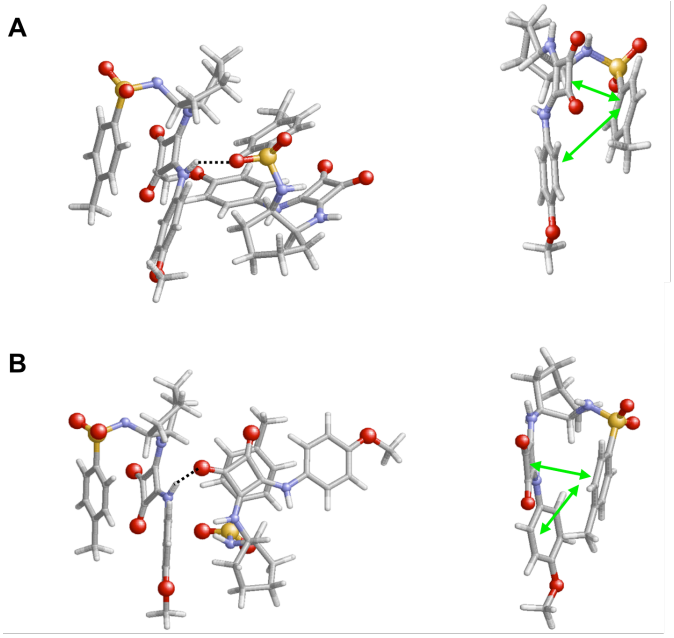

Figure S21. Representation of the two most stable complexes obtained for **8**: A) ΔE_i = –21.1 kcal mol^{-1} and B) ΔE_i = –20.4 kcal mol^{-1}. Intermolecular (*left*) and intramolecular (*right*) interactions are displayed for the complex and a single molecule of the complex, respectively. Hydrogen bonds are represented by black dashed lines and intramolecular π···π stacking interactions by green double arrows.

14.4. Minimum energy structure of a possible complex of **1** and MeOH

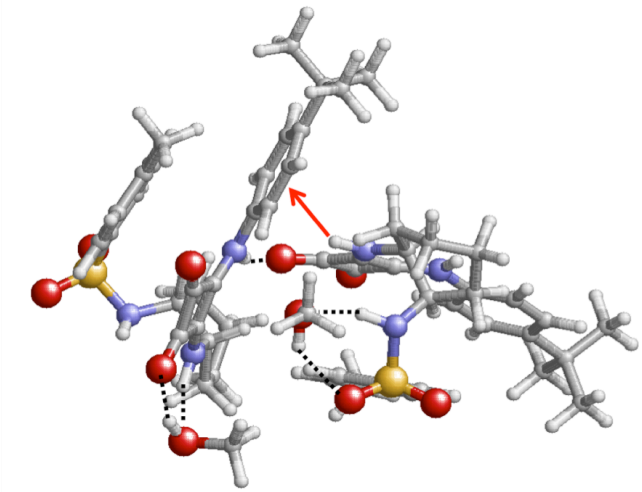

Figure S22. Representative minimum energy structure of a complex formed by two interacting molecules of **1** and two methanol molecules acting as a bridge. Intermolecular interactions are represented as follows: hydrogen bonds by black dashed lines and N–H···π interactions by read arrows.

15. Solvents and reagents used in this work

Solvent/reagent	Supplier, purity
Acetone	Sigma Aldrich, p.a.
Acetonitrile	Merck, p.a.
N-[(1*R*,2*R*)-2-Aminocyclohexyl]- -4-methylbenzenesulfonamide	Sigma Aldrich, 97%
(1*S*,2*R*)-(−)-*cis*-1-Amino-2-indanol	Sigma Aldrich, 99%
Aniline	Sigma Aldrich, 99.5%
3,5-Bis(trifluoromethyl)aniline	Alfa Aesar, 97%
Butane-1,4-diol	Sigma Aldrich, p.a.
Butan-1-ol	Merck, p.a.
Butan-2-ol	Merck, p.a.
4-*tert*-Butylaniline	Sigma Aldrich, 99%
Dibutylether	Fluka, >99 %
1,3-Dichlorobenzene	Aldrich, 98 %
Dichloroemethane	Sigma Aldrich, p.a.
3,4-Dimethoxy-3-cyclobutene-1,2-dione	Sigma Aldrich, 99%
3,5-Bis(trifluoromethyl)benzylamine	Alfa Aesar, 97%
3,5-Difluoroaniline	Acros, 98%
Diisopropyl azodicarboxylate	Sigma Aldrich, 98%
Dimethylsulfoxide	Fisher Chemicals, 99.8 %
Diphenyl phosphoryl azide	Sigma Aldrich, 95%
Ethane-1,2-diol	Sigma Aldrich, 99.8 %
Ethanol	Sigma Aldrich, >99.8 %
Ethoxyethane	Fluka, technical
Ethyl acetate	Fisher chemicals, p.a.
2-Furanmethanol	TCI, >98 %
Glycerol	Sigma Aldrich, >99.5 %
Hexan-1-ol	Sigma Aldrich, p.a.
1-Hexylamine	Merck, 98%
2-(2-Hydroxyethoxy)ethan-1-ol	TCI, >99.5 %
Methanol	VWR, p.a.
4-Methoxyaniline	Sigma Aldrich, 99%
2-(2-Methoxyyethoxy)ethanol	TCI, >98 %
Methylbenzene	VWR, p.a.
2-Methylbutan-1-ol	Sigma Aldrich, 99 %
2-Methylbutan-2-ol	Merck, p.a.
3-Methylbutan-2-ol	Sigma Aldrich, 98 %
2-Methylpentan-1-ol	TCI, >98 %
2-Methylpropan-1-ol	TCI, p.a.
2-Methylpropan-2-ol	Carl Roth, > 99 %
Pentane-1,5-diol	TCI, p.a.
Pentan-2-ol	VWR, p.a.
Phenylmethanol	Acros, 99%
(1*R*,2*R*)-*trans*-2-(1-Piperidinyl)- -cyclohexylamine	Sigma Aldrich, 97%
Propan-1-ol	Merck, p.a.
Propan-2-ol	Merck, p.a.
Quinine	Sigma Aldrich, 98%
Trichloromethane	VWR, p.a.
4-(Trifluoromethyl)aniline	Alfa Aesar, 98%
Triphenylphosphine	Sigma Aldrich, 95%